Electronic Supplementary Information

Evidence for triplet-state-dominated luminescence in bi-icosahedral superatomic molecular Au_{25} clusters

Masaaki Mitsui,*[a] Yuki Wada,[a] Ryoto Kishii,[a] Daichi Arima,[a] and Yoshiki Niihori[a]

[a] *Department of Chemistry, College of Science, Rikkyo University, 3-34-1, Nishiikebukuro, Toshima-ku, Tokyo, 171-8501, Japan.*

Corresponding author
*E-mail: mitsui@rikkyo.ac.jp

Contents

Chemicals

The following special-grade reagents were purchased from FUJIFILM Wako Pure Chemical Corp.: hydrogen tetrachloroaurate(III) tetrahydrate ($HAuCl_4{\cdot}4H_2O$, 99.0%), triphenylphosphine (PPh_3, 97.0+%), dichloromethane (DCM), methanol (MeOH), hexane, and tetrahydrofuran (THF). Sodium borohydride ($NaBH_4$, >95.0%), 2-phenylethanethiol (PET; >97.0%), 9,10-bis(phenylethynyl)anthracene (BPEA, >98.0%) and 3,3′-Diethylthiatricarbocyanine iodide (>98.0%) were purchased from Tokyo Chemical Industry Co., Ltd. Toluene and rubrene were purchased from Sigma-Aldrich Co. LLC. sodium hexafluoroantimonate(V) ($NaSbF_6$, 99%) was purchased from Fluorochem Ltd. Oxazine 1 perchlorate (Oxazine, 99.0%) was purchased from MedChemExpress LLC. *meso*-Tetraphenyl-tetrabenzoporphine palladium complex (PdTPTBP, >97%) was purchased from AdipoGen Life Sciences, Inc. (KOM). All chemicals are used as received. Ultrapure water (≥18.2 MΩcm) was produced by a Direct-Q UV distillation system.

Synthesis

The synthesis of $[Au_{25}(PPh_3)_{10}(PET)_5Cl_2]^{2+}$ (hereafter abbreviated as Au_{25}-rod) was performed by slightly modifying a reported method for preparing ultra-pure Au_{25} clusters.[1] First, 103.0 mg (250 µmol) of $HAuCl_4{\cdot}4H_2O$ was dissolved in 8 mL of ethanol, 180 mg (686 µmol) of PPh_3 was added, and the solution was stirred at room temperature for 15 min. The color of the solution turned from yellow to transparent, and a white solid precipitated. Subsequently, the solvent was removed, and the white solid was dissolved in 8 mL of toluene. When an ethanol solution of sodium borohydride (26 mg/5 mL) was added to this toluene solution at once, the solution turned black. After stirring for 2 h, the solvent was removed from the solution, which turned blackish red, using a rotary evaporator under temperature conditions of 50 °C, and the remaining black-red solid was dissolved in 20 mL of DCM. Only the solution portion was removed by centrifugation, and 300 µL (2.24 mmol) of phenylethanethiol was added and stirred in a thermostatic bath at 40°C. After 96 h, an excess amount of hexane was added to the yellowish solution to precipitate the crude product, and then the supernatant was removed. The crude product was washed five times with a mixture of hexane and DCM (9 : 1 by volume), then dissolved in methanol, an excess amount of $NaSbF_6$ was added, and only the supernatant was removed. The solvent was evaporated and finally washed with a mixture of methanol and water (2 : 8 by volume) to obtain the desired product.

Sample Preparation

Unless otherwise noted, all sample solutions were placed in a quartz cell with an optical path length of 1 cm, sealed with a rubber cap, and thoroughly deoxygenated by bubbling with high-purity Ar gas (> 99.999%) before optical measurements. The sample solution cell thus deoxygenated was also purged or bubbled by constant flow of Ar gas during the measurements.

Absorption and photoluminescence measurements

UV-visible absorption spectra were recorded on a Lambda 650 spectrometer (Perkin-Elmer). Photoluminescence (PL) spectra were recorded using a SpectraPro 2300i polychromator coupled with a liquid-nitrogen-cooled charge coupled device (CCD) camera (Spec-10:100B/LN, Roper Scientific) or a fiber optic spectrometer (USB4000, Ocean Optics). For PL spectral measurements, a linearly polarized continuous wave (cw) diode laser with a wavelength of 640 nm (CUBE 640-40C, Coherent) or 785 nm (LDM785, Thorlabs) was used as the excitation source. Meanwhile, a 441, 478, or 634 nm picosecond pulsed laser (pulse width 40-80 ps, PiL044X, PiL048X or PiL063X, Advanced Laser Diode System) was used to measure the PL lifetime of the clusters and organic emitter molecules. All the signals, including the synchronization of pulse laser and an avalanche photodiode (APD, SPCM-AQRH-61, Perkin-Elmer), were fed to the time-correlated single photon counting (TC-SPC) card (TimeHarp 260, PicoQuant) operating in time-tagged and time-resolved modes. Data acquisition and fluorescence decay analysis were performed using the SymPhoTime 64 (PicoQuant) software. Experimental setup for the delayed fluorescence decay measurements has been already reported elsewhere.[2] In brief, a 640 nm cw-laser periodically blocked at 400–800 Hz by an optical chopper (MC2000B controller, MC1F10HP blade, Thorlabs) was used as an excitation source. Based on the measurements of scattered light in the rotational frequency range, the time resolution was estimated to be a few microseconds, which is sufficiently shorter than the observed delayed fluorescence decay times of the BPEA and rubrene emitters (> 100 μs). The emission signal was detected by an APD (APD410A/M, Thorlabs) and monitored by a digital storage oscilloscope (GDS1062A, 60MHz, Chip One Stop) while synchronized with the chopper. The decay profiles were averaged at 256 times and stored in the oscilloscope.

Transient absorption spectroscopy

Transient absorption (TA) measurements under deaerated condition were performed using a picosecond transient absorption spectroscopy system (picoTAS, UNISOKU Co., Ltd.) based on the randomly interleaved pulse train method.[3] The pump source is a picosecond Nd:YAG laser (355 nm, EKSPLA PL-2210A, 1 kHz, fwhm = 25 ps) equipped with an optical parametric generator (EKSPLA PG403, 410−700 nm, 50 μJ/pulse @500 nm), and the probe light source is a supercontinuum radiation source (SMHP-20.2, Leukos, 20 MHz, fwhm = 50−100 ps, 410−2000 nm). The time resolution of the system is estimated to be 80−100 ps from 10−90% rise time.[3] All TA measurements were performed at room temperature, under deaerated conditions, using a quartz cell with an optical path length of 2 mm.

Theoretical calculations

Density functional theory (DFT) and time-dependent (TD)-DFT calculations were implemented with the program Gaussian 16 (ES64L-G16, RevB.01).[4] For reducing CPU cost, all the PPh_3 and SC_2H_4Ph ligands in the clusters were replaced with $P(CH_3)_3$ and SH ligands. Geometric structure of $[Au_{25}(P(CH_3)_3)_{10}(SH)_5Cl_2]^{2+}$ in the ground state was optimized using the BP86 functional[5] with the basis sets of def2-SV(P)[6] for Au atom and 6-31G(d,p) for H, C, P, S, and Cl atoms,[7] and SDD pseudopotentials with scalar relativistic effects were included.[8] Note that no symmetry constraints were added during the structural optimization. Furthermore, harmonic vibrational frequency analysis was performed for the optimized geometry, confirming no imaginary frequencies. The optimized structure and corresponding molecular orbitals (MOs) are shown in Fig. S5. Using these optimized structures, vertical transition energies of $S_0 \rightarrow S_n$ (n = 1–200) and $S_0 \rightarrow T_n$ (n = 1–10) were calculated using the TD-B3LYP functional.[9–11] In this calculation, the basis sets of def2-SV(P) for Au atom and 6-31G(d,p) for H, C, P, S, and Cl atoms, and SDD pseudopotentials were also used. It has been previously confirmed that the abovementioned calculation levels reproduce relatively well the electronic structure of ligand-protected noble metal clusters.[2,12,13] The molecular geometries and MOs were constructed using Avogadro 1.2.0.

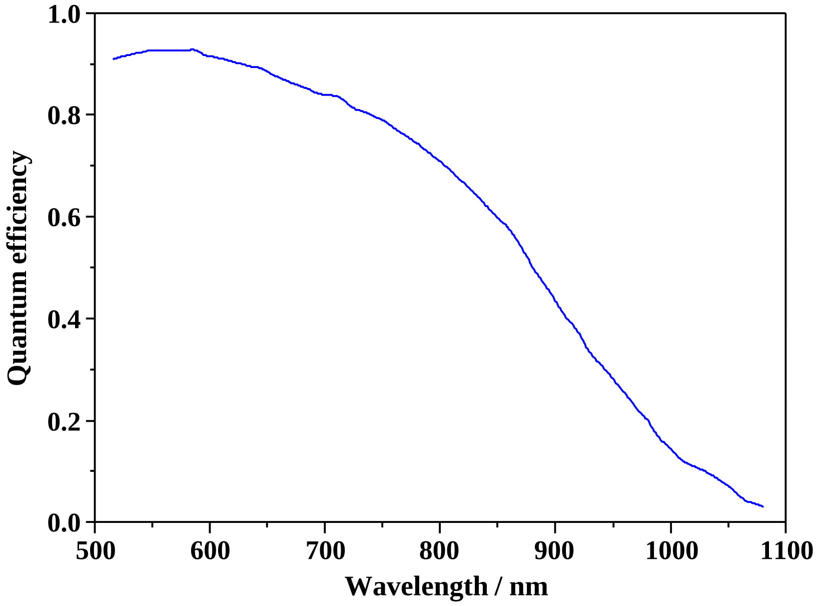

Fig. S1 Wavelength dependence of the quantum efficiency of the photocathode of the liquid nitrogen cooled CCD device (Spec-10:100B/LN, Roper Scientific) used in this study

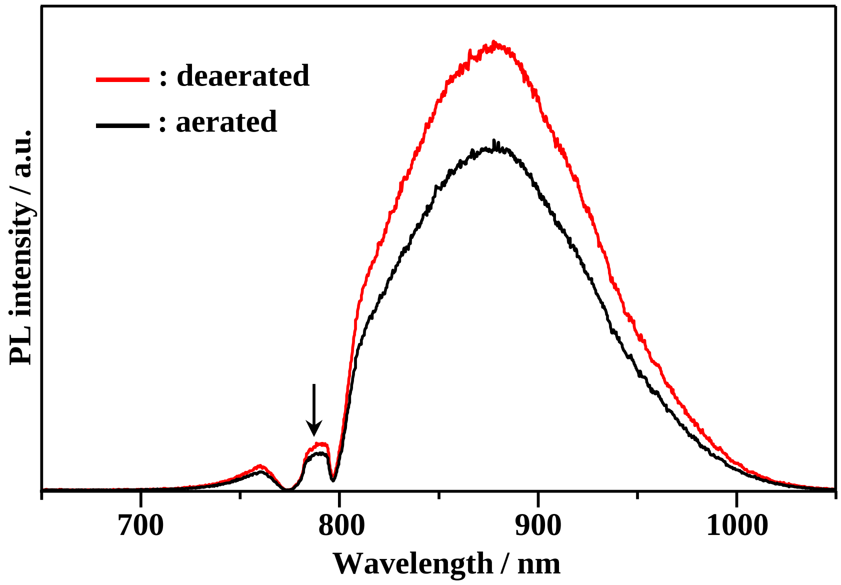

Fig. S2 PL spectra of Au_{25}-rod (10.5 µM) in deaerated and aerated THF (excitation wavelength λ_{ex} = 785 nm indicated by the down arrow).

Table S1. PL lifetimes of Au_{25}-rod (10 µM) in aerated and deaerated THF.

Condition	τ_I / µs	f_I (%)	τ_{II} / µs	f_{II} (%)
aerated	0.76	4.5	3.03	95.5
deaerated	0.80	3.6	3.36	96.4

Table S2. PL lifetimes and their fractional populations of Au_{25}-rod in deaerated THF.

[Au_{25}-rod] / µM [a]	sample [b]	τ_I / µs	f_I (%)	τ_{II} / µs	f_{II} (%)	χ^2
0.10	A	0.79	2.3	3.64	97.7	1.04
	B	0.47	3.8	3.53	96.2	1.03

[a] The cluster concentration was set low (i.e., 0.10 µM) in order to shift the equilibrium in the direction of aggregate formation as much as possible. [b] Sample A is the as-synthesized $[Au_{25}(PPh_3)_{10}(PET)_5Cl_2](SbF_6)_2$ dissolved in THF, whereas Sample B corresponds to the Sample A with a large excess of SbF_6^-.

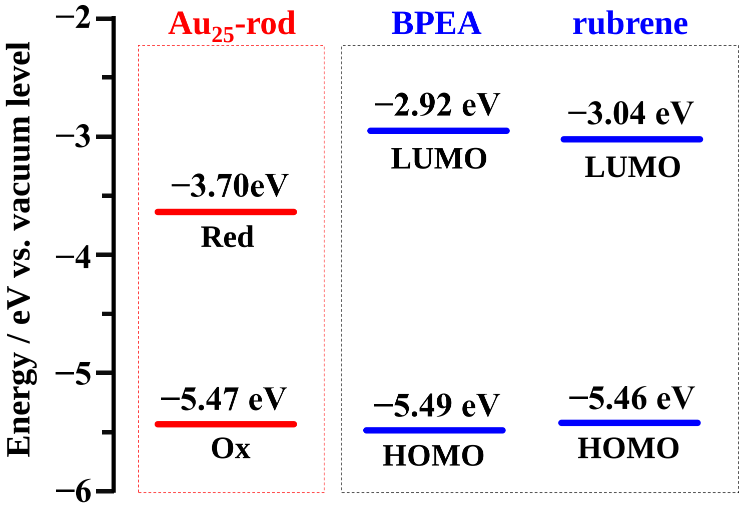

Fig. S3 Redox potentials of Au_{25}-rod sensitizer[14] and BPEA[15] and rubrene[16] emitters. In these sensitizer–emitter combinations, the redox potential relationship is such that neither electron transfer nor hole transfer is likely to occur when the Au_{25}-rod cluster are photoexcited.

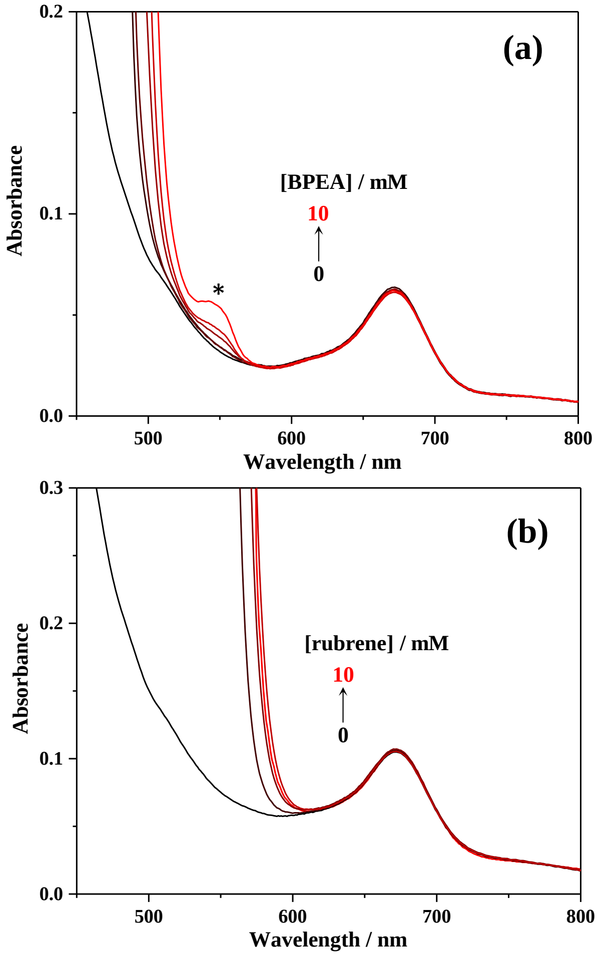

Fig. S4 Absorption spectra of Au_{25}-rod with (a) BPEA (0–10 mM) and (b) rubrene (0–10 mM) in aerated THF. The peak with asterisk in panel a, which begin to appear when the BPEA concentration exceeds ~5 mM, are assigned to emission from BPEA aggregates. We note that Tyndall scattering was clearly observed at 10 mM BPEA concentration.

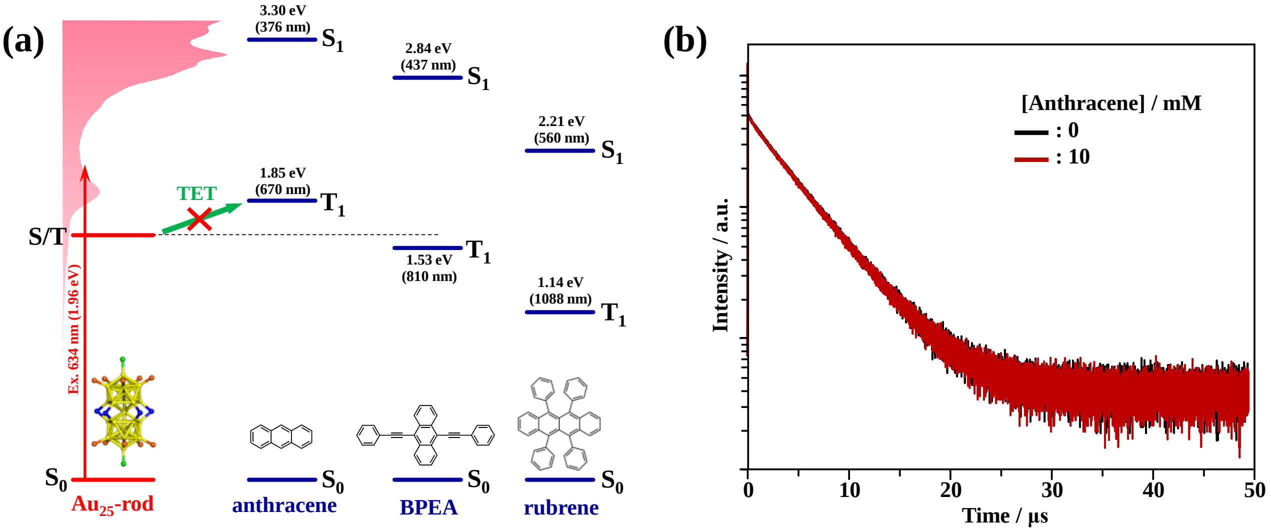

Fig. S5 a) Energy-level diagram of the Au_{25}-rod sensitizer combined with an anthracene, BPEA or rubrene emitter. The TET from Au_{25}-rod to anthracene is an endothermic process of ~0.3 eV. b) PL decay profiles of Au_{25}-rod with anthracene (0 or 10 mM) in deaerated THF (excitation wavelength λ_{ex} = 634 nm).

Table S3. PL lifetimes of Au_{25}-rod (10.5 µM) and anthracene (0 or 10 mM) in aerated and deaerated THF.

[Anthracene] / mM	τ_I / µs	f_I (%)	τ_{II} / µs	f_{II} (%)
0	0.75	3.6	3.43	96.4
10	0.79	3.4	3.41	96.6

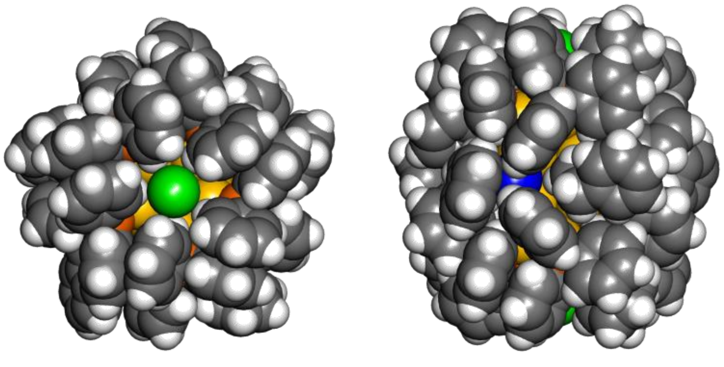
Top view

Side view

Fig. S6 Geometrical structure (top view and side view) of Au_{25}-rod, which is drawn based on ref. 17.

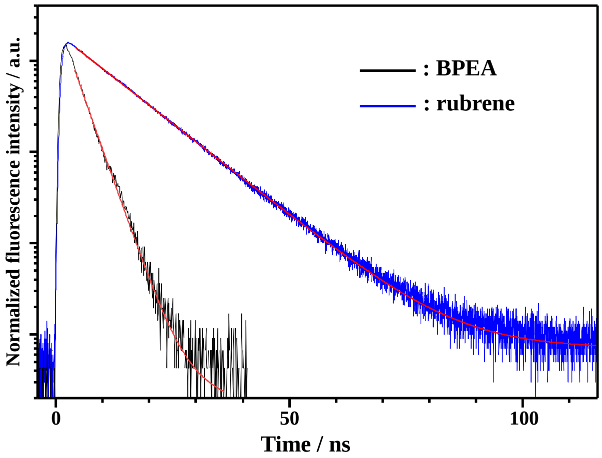

Fig. S7 Fluorescence decay curves of BPEA and rubrene (~1 μM) in deaerated THF (λ_{ex} = 478 nm). The red lines are single-exponential fits.

Evaluation of the UC state formation yield (Φ_{UCs}) by relative method

The uncorrected TF-UC efficiency (Φ_{UC}), determined by conventional relative estimation using the following equation:

$$\Phi_{\mathrm{UC}} = \frac{I_{\mathrm{r}}\left(1-10^{-A_{\mathrm{r}}(\lambda_{\mathrm{ex}})}\right)}{I_{\mathrm{s}}\left(1-10^{-A_{\mathrm{s}}(\lambda_{\mathrm{ex}})}\right)} \frac{\int F_{\mathrm{s}}(\lambda_{\mathrm{em}})\,\mathrm{d}\lambda_{\mathrm{em}}}{\int F_{\mathrm{r}}(\lambda_{\mathrm{em}})\,\mathrm{d}\lambda_{\mathrm{em}}} \frac{{n_{\mathrm{s}}}^2}{{n_{\mathrm{r}}}^2} \Phi_{\mathrm{f}}^{\mathrm{r}}, \tag{S1}$$

where $\Phi_{\mathrm{f}}^{\mathrm{r}}$ represents the known fluorescence quantum yield of the reference dye, A, F, and I represent the absorbance at the excitation wavelength (λ_{ex}), the PL intensity, and excitation laser intensity, respectively, and n is the refractive index of the corresponding solvent. Oxazine 1 perchlorate ($\Phi_{\mathrm{f}}^{\mathrm{r}}$ = 0.141 ± 0.008 in methanol[18]) and 3,3′-Diethylthiatricarbocyanine iodide ($\Phi_{\mathrm{f}}^{\mathrm{r}}$ = 0.22 in methanol[19]) was used as a reference dye for 640 nm excitation. However, the Φ_{UC} is not necessarily a quantity unique to the TF-UC system, as it is strongly affected by several loss factors depending on the sample and experimental conditions, as mentioned below.

As shown in Fig. S8, the UC state formation yield (Φ_{UCs}), i.e., the number of the excited singlet state of emitter ($\#^1\mathrm{E}^*$) generated per the number of photons absorbed by the sensitizer ($\#^1\mathrm{S}^*$), can be experimentally evaluated by the following equation:[20]

$$\Phi_{\mathrm{UCs}} = \frac{\Phi_{\mathrm{UC}}}{\Phi_{\mathrm{out}}\left(1-\Phi_{\mathrm{q}}\right)\Phi_{\mathrm{f}}} \tag{S2}$$

where Φ_{out} and Φ_{q} represent the output coupling yield, which is the fraction of detected photons ($\#h\nu_{\mathrm{obs}}$) out of the UC photons emitted from the emitter ($\#h\nu_{\mathrm{f}}$), and the quenching yield of $^3\mathrm{E}^*$ by the sensitizer, respectively.

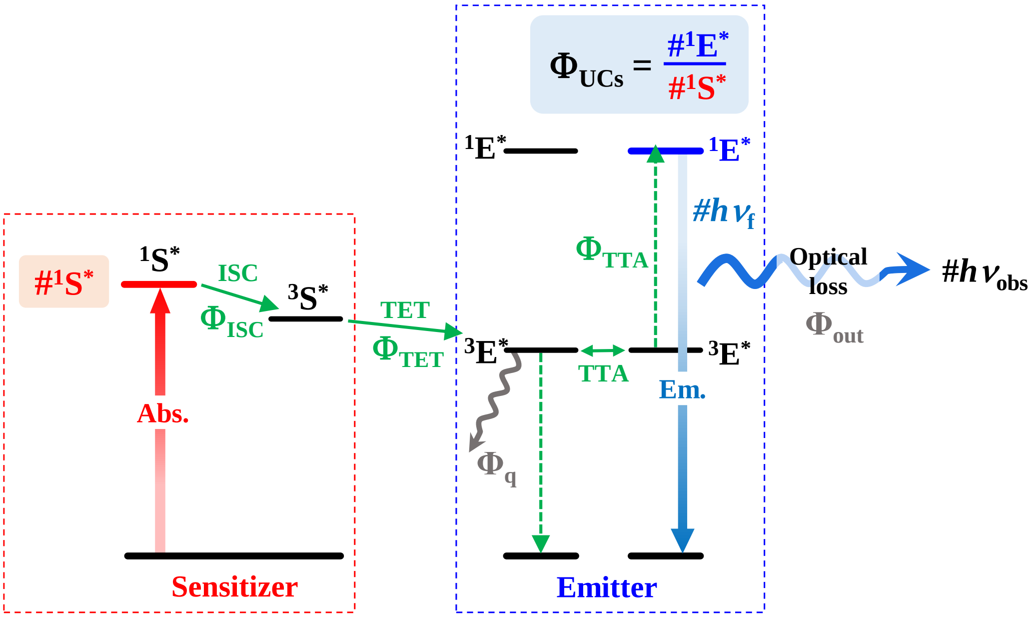

Fig. S8 Schematic diagram of TF-UC occurring in the system of a sensitizer–emitter pair.

The details of the evaluation procedure for Φ_{out} and Φ_q have already been reported in ref. 2, and will be briefly explained below. The Φ_{out} can be evaluated by the following equation:

$$\Phi_{out} = \frac{\int F_0(\lambda) \cdot 10^{-\frac{A(\lambda)}{2}} \mathrm{d}\lambda}{\int F_0 \, (\lambda) \mathrm{d}\lambda}. \tag{S3}$$

where $F_0(\lambda)$ is the emission intensity at a wavelength λ in a dilute solution. The absorbance at a wavelength λ of the UC solution, $A(\lambda)$, was measured under an optical path length of 1.0 cm. In the TF-UC measurement, since the excitation laser is focused on the center of the 1.0 × 1.0 cm cuvette, the optical path length of the emitted photons is 0.5 cm, and the actual observed emission intensity can be represented as $F_0(\lambda) \cdot 10^{-A(\lambda)/2}$. The fluorescence spectrum in dilute solution $F_0(\lambda)$, transmittance curve $10^{-A(\lambda)/2}$, and corrected fluorescence spectrum $F_0(\lambda) \cdot 10^{-A(\lambda)/2}$ of BPEA and rubrene are shown in Fig. S9. In the Au_{25}/rubrene system, the measured UC fluorescence spectrum and the corrected spectrum show an excellent agreement, while in the Au_{25}/BPEA system, a distinct difference was observed between them. This is because $^1BPEA^*$ generated by triplet-triplet annihilation in a solution of high concentration (10 mM) forms excimer and its emission is observed (peak labeled with asterisk).[21]

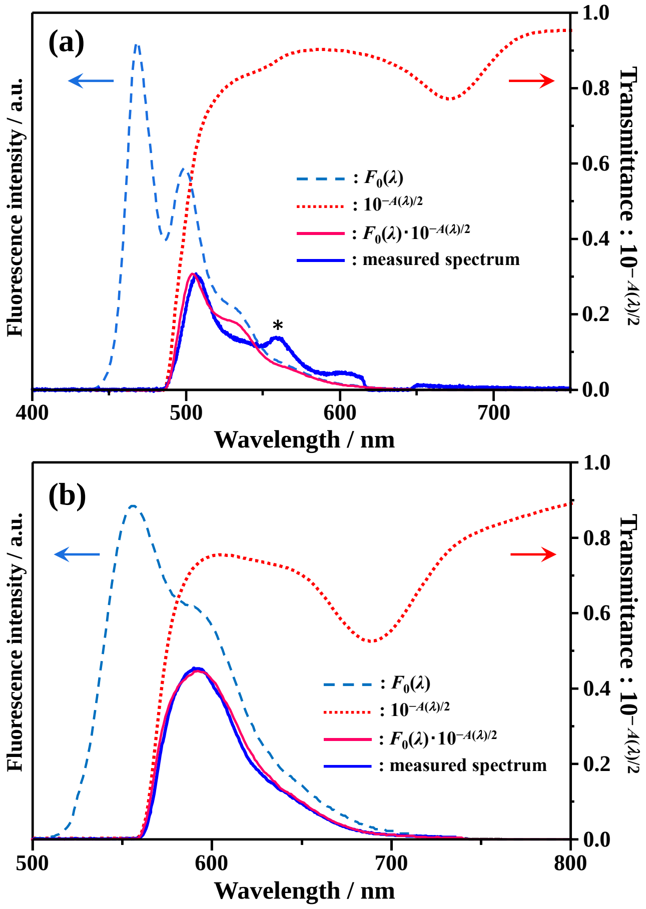

Fig. S9 Fluorescence spectrum $F_0(\lambda)$ (dashed line) of (a) BPEA (1 μM) and (b) rubrene (M) in THF and transmittance curve (dotted line), given by $10^{-A(\lambda)/2}$, of a mixed solution containing (a) Au_{25}-rod (13.3 μM)/BPEA (10 mM) and (b) Au_{25}-rod (40 μM)/rubrene (10 mM). The corrected fluorescence spectrum (solid pink line) obtained by multiplying the fluorescence spectrum in dilute solution ($F_0(\lambda)$) by the transmittance curve ($10^{-A(\lambda)/2}$) is in good agreement with the measured UC spectrum (solid blue line).

To obtain the value of Φ_q, the emitter triplet lifetime (τ_T) for each sensitizer concentration was determined by fitting the UC emission decay curve, $I(t)$, using the following equation:[22]

$$I(t) = I(0)\left(\frac{1-\beta}{\exp(t/\tau_T)-\beta}\right)^2 \tag{S4}$$

where

$$\beta = \frac{2k_{TTA}[^3E^*]_0}{1/\tau_T + 2k_{TTA}[^3E^*]_0} \qquad (0 < \beta < 1). \tag{S5}$$

Figs. S10a and 10b shows the TF-UC emission decay curves obtained at different sensitizer concentrations and the extracted values of τ_T and β are summarized in Table S4 and S5. As shown in Figs. S10c and 10d, the values of τ_T were plotted against sensitizer concentration, [sen], to generate Stern–Volmer plots described by the following relationship:

$$\frac{1}{\tau_\mathrm{T}} = \frac{1}{\tau_\mathrm{T0}} + k_\mathrm{q}[\mathrm{sen}]. \tag{S6}$$

Additionally, the quenching efficiency (Φ_q) is calculated by

$$\Phi_\mathrm{q} = \frac{k_\mathrm{q}\tau_\mathrm{T0}[\mathrm{sen}]}{1 + k_\mathrm{q}\tau_\mathrm{T0}[\mathrm{sen}]}. \tag{S7}$$

The obtained parameters (k_q and τ_T0) in Eq. S7 are shown in Fig. S10b and S10d.

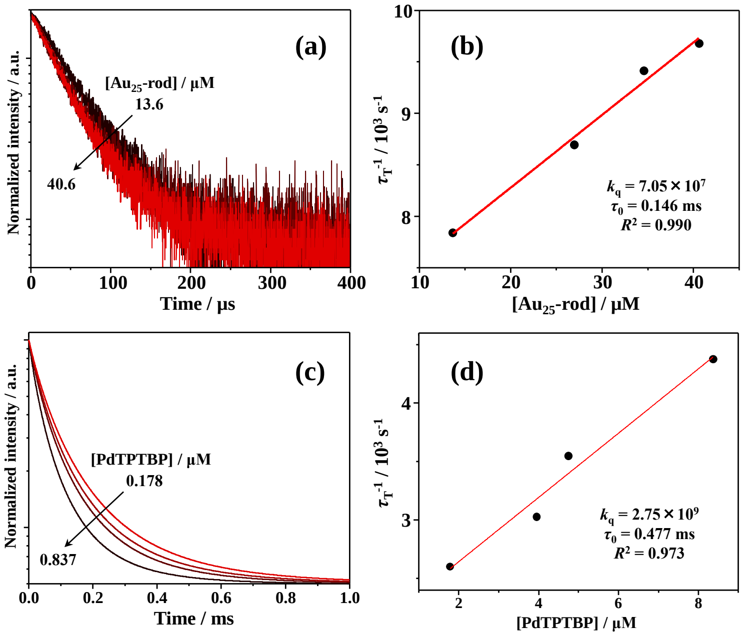

Fig. S10 Delayed fluorescence decay curves and corresponding Stern–Volmer plots (Eq. S6) of solutions containing different concentrations of (a,b) $\mathrm{Au_{25}}$-rod or (c,d) PdTPTBP with 10 mM BPEA excited at 640 nm with excitation intensity of 10.4 and 30.6 Wcm^{-2}, respectively.

Table S4. Triplet lifetimes of BPEA (10 mM) in deaerated THF containing different $\mathrm{Au_{25}}$-rod sensitizer concentrations.

[$\mathrm{Au_{25}}$-rod] / µM	τ_T / µs	β
12.4	127.5	0.252
16.9	115.0	0.382
21.4	106.2	0.343
25.5	103.3	0.230

Table S5. Triplet lifetimes of BPEA (10 mM) in deaerated THF containing different PdTPTBP sensitizer concentrations.

[PdTPTBP] / μM	τ_{T} / μs	β
0.178	384.1	0.855
0.395	330.2	0.852
0.474	281.7	0.843
0.837	228.4	0.857

Table S6. Measured and corrected upconversion quantum yields (at a maximum of 50%) and their related parameters for the Au_{25}-rod (13.3 μM) and BPEA in deaerated THF.

λ_{ex} / nm[a]	sensitizer	emitter	[E] / mM	Φ_{TET}	Φ_{UC} (%)[c]	Φ_{out}[d]	$1-\Phi_{\mathrm{q}}$[e]	f_2[f]	Φ_{UCg} (%)[g]
640	Au_{25}-rod	BPEA	10	0.249[b]	0.665	0.357	0.880	0.0691	1.9
	PdTPTBP			1.00	15.2	0.470	0.811	0.336	32.3

[a] Excitation power density was set at 10 $\mathrm{Wcm^{-2}}$ for the Au_{25}-rod and BPEA system. [b] Triplet energy transfer efficiency (Φ_{TET}) was determined by the analysis of the Stern-Volmer plot obtained from the PL spectra of Au_{25}-rod shown as the inset of Fig. 2b. [c] Oxazine 1 (Φ_{f} = 0.141 ± 0.008 in methanol[18]) was used as the reference dye, and the values were calculated by the relative method using Eq. S1. [d] Output coupling yield calculated using Eq. S3. [e] Calculated using Eq. S7. [f] Calculated using Eq. 4. [g] Internal TTA-UC yield obtained using $\Phi_{\mathrm{UC}} / \Phi_{\mathrm{out}}$

Table S7. Measured and corrected upconversion quantum yields (at a maximum of 50%) and their related parameters for the Au_{25}-rod (6.7 μM) and rubrene in deaerated THF.

λ_{ex} / nm[a]	sensitizer	emitter	[E] / mM	Φ_{TET}[b]	Φ_{UC} (%)[c]	Φ_{out}[d]	Φ_{UCg} (%)[e]
785	Au_{25}-rod	rubrene	10	0.75	0.057	0.456	0.13

[a] Measured at an excitation power density of 5.54 $\mathrm{Wcm^{-2}}$. [b] Triplet energy transfer efficiency (Φ_{TET}) was determined by the analysis of the Stern-Volmer plot obtained from the PL spectra of Au_{25}-rod shown as the inset of Fig. 2c. [c] 3,3′-Diethylthiatricarbocyanine iodide (Φ_{f} = 0.22 in methanol[19]) was used as the reference dye, and the values were calculated by the relative method using Eq. S1. [d] Output coupling yield calculated using Eq. S3. [e] Internal TTA-UC yield obtained using $\Phi_{\mathrm{UC}} / \Phi_{\mathrm{out}}$

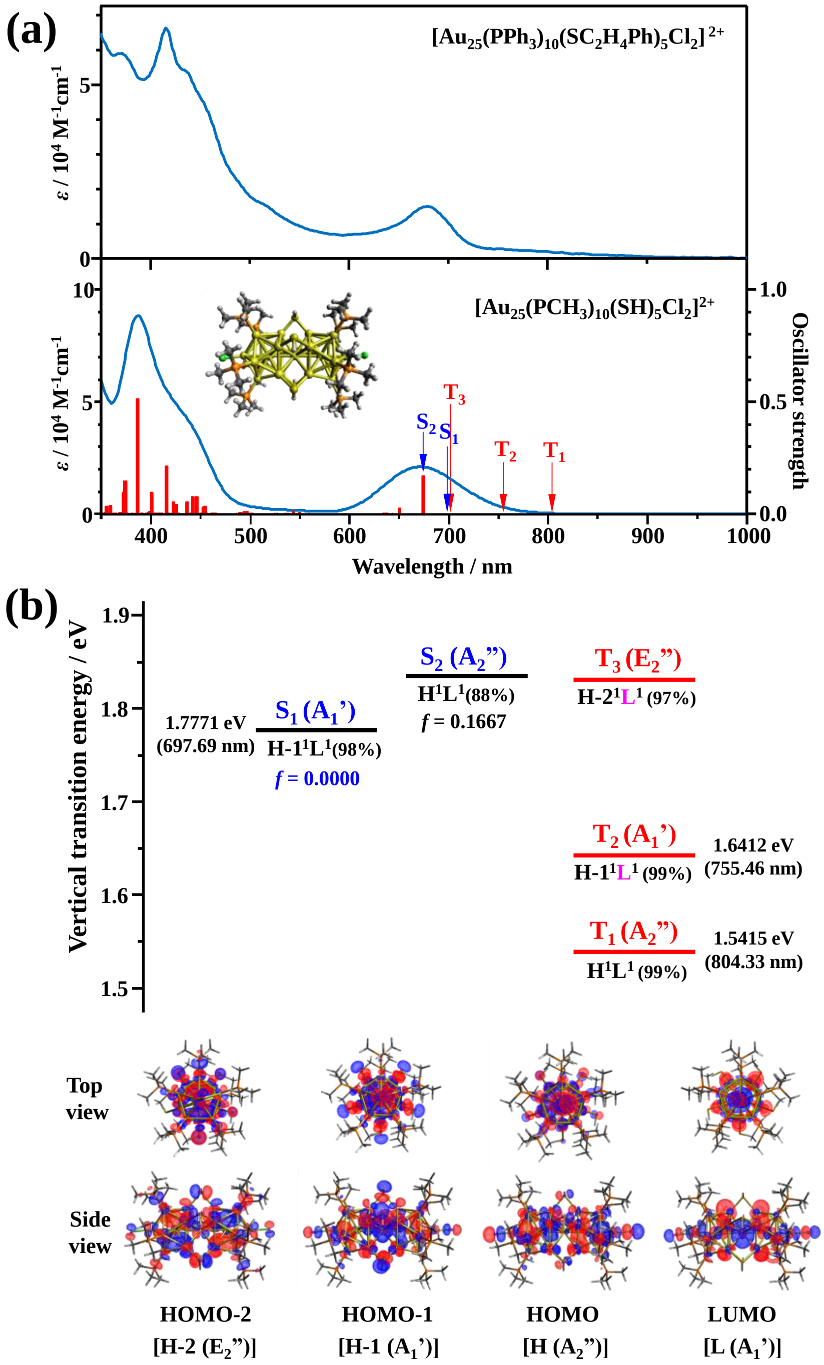

Fig. S11 (a) The experimental UV–vis absorption spectrum of Au_{25}-rod in THF (upper panel) and the TD-DFT calculated bar spectrum of $[Au_{25}(P(CH_3)_3)_{10}(SH)_5Cl_2]^{2+}$ (lower panel). The vertical lines provide the oscillator strength of each $S_0 \rightarrow S_n$ transition. The down arrows indicate the $S_0 \rightarrow T_n$ transition energies ($n = 1$−3). The computed spectrum was obtained by a convolution of the bar spectra with a Gaussian line shape ($\sigma = 0.12$ eV) to account for broadening effects. (b) TD-DFT calculated energy diagram of $S_{1,2}$ and $T_{1\text{–}3}$ states of $[Au_{25}(P(CH_3)_3)_{10}(SH)_5Cl_2]^{2+}$ (upper panel). The vertical transition energies are obtained for the equilibrium geometry of the S_0 state. The electronic configuration of each electronic state is also shown using the notations HOMO-2 (H-2), HOMO-1

(H-1), HOMO (H), LUMO (L). Also shown are the irreducible representation for each MO and electronic state, assuming that the S_0 structure belongs to the D_{5h} point group. Note that as mentioned earlier, the symmetry constraint was indeed not imposed in the actual geometrical optimization of S_0. It should be emphasized that the electronic transition between S_1(A_1’) and S_0(A_1’) is symmetrically forbidden and thus its oscillator strength (*f*) is zero.

References

1. M. Galchenko, R. Schuster, A. Black, M. Riedner, C. Klinke, *Nanoscale,* 2019, **11**, 1988.
2. Y. Niihori, Y. Wada, M. Mitsui, *Angew. Chem. Int. Ed.*, 2021, **60**, 2822.
3. T. Nakagawa, K. Okamoto, H. Hanada, R. Katoh, *Opt. Lett*., 2016, **41**, 1498.
4. Gaussian 16, Revision B.01, Frisch, M. J.; Trucks, G. W.; Schlegel, H. B.; Scuseria, G. E.; Robb, M. A.; Cheeseman, J. R.; Scalmani, G.; Barone, V.; Petersson, G. A.; Nakatsuji, H.; et al. Gaussian, Inc., Wallingford CT, 2016.
5. A. D. Becke, *Phys. Rev. A*, 1988, **38**, 3098.
6. F. Weigend, R. Ahlrichs, *Phys. Chem. Chem. Phys.*, 2005, **7**, 3297.
7. M. M. Francl, W. J. Pietro, W. J. Hehre, J. S. Binkley, M. S. Gordon, D. J. DeFrees, J. A. People, *J. Chem. Phys.*, 1982, **77**, 3654.
8. D. Andrae, U. Häußermann, M. Dolg, H. Stoll, H. Preuß, Theor. *Chim. Acta*, 1990, **77**, 123.
9. A. D. Becke, *J. Chem. Phys.*, 1993, **98**, 1372.
10. C. Lee, W. T. Yang, R. G. Parr, *Phys. Rev. B*, 1988, **37**, 785.
11. E. Runge, E. K. U. Gross, *Phys. Rev. Lett.*, 1984, **52**, 997.
12. Y. Niihori, N. Takahashi, M. Mitsui, *J. Phys. Chem. C*, 2020, **124**, 5880.
13. X.-Y. Xie, P. Xiao, X. Cao, W.-H. Fang, G. Cui, M. Dolg, *Angew. Chem. Int. Ed.*, 2018, **57**, 9965.
14. S. Matsuo, S. Yamazoe, J.-Q. Goh, J. Akola, T. Tsukuda, *Phys. Chem. Chem. Phys.*, 2016, **18**, 4822.
15. J. Liu, J. Liu, Z. Zhang, C. Xu, Q. Li, K. Zhou, H. Dong, X. Zhang, W. Hu, *J. Mater. Chem. C*, 2017, **5**, 2519.
16. F. Anger, T. Breuer, A. Ruff, M. Klues, A. Gerlach, R. Scholz, S. Ludwig, G. Witte, F. Schreiber, *J. Phys. Chem. C*, 2016, **120**, 5515.
17. Y. Shichibu, Y. Negishi, T. Watanabe, N. K. Chaki, H. Kawaguchi, T. Tsukuda, *J. Phys. Chem. C*, 2007, **111**, 7845.
18. K. Rurack, M. Spieles, *Anal. Chem.*, 2011, **83**, 1232.
19. M. R. V. Sahyun, N. Serpone, *J. Phys. Chem. A*, 1997, **101**, 9877.
20. Y. Zhou, F. N. Castellano, T. W. Schmidt, K. Hanson, *ACS Energy Lett*., 2020, **5**, 2322.
21. Y. J. Bae, D. Shimizu, J. D. Schultz, G. Kang, J. Zhou, G. C. Schatz, A. Osuka, M. R. Wasielewski, *J. Phys. Chem. A*, 2020, **124**, 8478.
22. Y. Y. Cheng, B. Fückel, T. Khoury, R. G. C. R. Clady, M. J. Y. Tayebjee, N. J. Ekins-Daukes, M. J. Crossley, T. W. Schmidt, *J. Phys. Chem. Lett.*, 2010, **1**, 1795.